International Journal of Heat and Mass Transfer 52 (2009) 1875–1886

Contents lists available at ScienceDirect

International Journal of Heat and Mass Transfer

journal homepage: www.elsevier.com/locate/ijhmt

# Heat transfer model for small-scale spark-ignition engines

Yuh-Yih Wu [a,*], Bo-Chiuan Chen [a], Feng-Chi Hsieh [b], Cheng-Ting Ke [a]

[a] Department of Vehicle Engineering, National Taipei University of Technology, 1, Sector 3, Chung-Hsiao E. Road, Taipei 106, Taiwan, ROC
[b] Hua-Chuang Automobile Information Technical Center (HAITEC), 8F., No. 3, Zhongxing Road, Xindian City, Taiwan, ROC

ARTICLE INFO

*Article history:*
Received 19 March 2008
Received in revised form 18 September 2008
Available online 8 December 2008

*Keywords:*
Engine heat transfer model
Stanton number
Spark-ignition engine
Heat flux

ABSTRACT

A heat transfer model for small-scale spark-ignition engines has been proposed by authors in previous study. However, that model was developed based on experimental data of one engine, it may not be so accurate for others. In order to improve the accuracy of predicted heat transfer rate for different engines, a modified heat transfer model using Stanton number based on two engines is proposed. Prediction results of instantaneous heat flux, global heat transfer, heat release rate, and cylinder pressure based on the proposed model are compared with the experimental results of three engines and prediction results of previous model. It is found that the proposed model has prediction results closer to the measured data than the previous models at the most engine operation conditions.



## 1. Introduction

The heat transfer model can be used to predict the engine heat transfer rate, which is very important for thermal load analysis, combustion performance prediction, and cycle simulation. Most investigations of heat transfer in spark ignition (S.I.) engines are large-scale ones. Oguri [1] used Eichelberg's model to predict the heat transfer rate of a 1400 c.c. S.I. engine, yielding predicted results that agreed with the experimental results for the expansion stroke, but not for the compression stroke. This might be because the model was established for diesel engines and was not suitable for S.I. engines. Alkidas [2,3] measured the instantaneous heat flux on the cylinder head of an 820 c.c. four-stroke S.I. engine and found that it could be affected by the engine speed, air–fuel ratio, and volumetric efficiency. Alkidas and Suh [4] investigated the effects of swirl or tumble motion on the heat transfer and combustion characteristics of a single-cylinder four-valve 400 c.c. S.I. engine. It was found that increasing swirl or tumble motions might raise the peak rate of heat release, the local surface temperature, and heat flux, on the cylinder head. Shayler et al. [5] utilized two methods to obtain the instantaneous heat flux of the combustion chamber. In the first method, the first law of thermodynamics was applied to calculate the heat transfer rate, but the results were not accurate due to uncertain gas properties. In the second method, the heat transfer rates were calculated based on Woschni's, Annand's, and Eichelberg's experimental models. It was found that Eichelberg's model could produce prediction results closest to the experimental data.

Previous studies have focused on developing heat transfer models for large-scale engines. However, the heat transfer characteristics of large-scale and small-scale engines are quite different. For large-scale S.I. engines, about one-third of the fuel energy is transformed to heat loss from the cylinder body. But for a small-scale 125 c.c. two-stroke S.I. engine, Franco and Martorano [6] found that approximately 50% of the fuel energy is converted to heat loss, which is much higher than that of large-scale S.I. engines. Since the heat transfer characteristics of small-scale engine are different from that of large-scale engine, the authors of this paper [7] had ever proposed a heat transfer model specific for four-stroke small-scale S.I. engines using Stanton number. However, that model was developed based on experimental data of one engine, it may not be so accurate for others.

In order to improve the accuracy of the predicted heat transfer rate for different scooter engines, a heat transfer model also using the Stanton number is proposed and based on two 125 c.c. air-cooled four-stroke S.I. engines. The remainder of this paper is organized as follows. Section 2 introduces previous heat transfer model. The heat flux obtained from the measured temperatures is then used to establish the heat transfer model in Section 3. The heat transfer model is used for engine simulation and the engine model is described in Section 4. Simulation results of cylinder pressure are compared with the experimental results of three engines in Section 5. Finally, conclusions are made in Section 6.

## 2. Heat transfer model

The heat transfer rate $\dot{Q}_{ht}$ from the flowing gas to the combustion chamber wall is dominated by the forced convection [7,8] and can be expressed as:

* Corresponding author. Tel.: +886 2 27712171 3620; fax: +886 2 27314990.
*E-mail address:* cyywu@ntut.edu.tw (Y.-Y. Wu).

0017-9310/$ - see front matter © 2008 Elsevier Ltd. All rights reserved.
doi:10.1016/j.ijheatmasstransfer.2008.10.015

**Nomenclature**

| | |
|---|---|
| $A$ | area of the heat absorbing surface ($m^2$) |
| $A_n$,$B_n$ | Fourier coefficients |
| $A_{th}$ | cross-sectional area of throttle body ($m^2$) |
| $B$ | Bore diameter (m) |
| $C_d$ | discharge coefficient |
| $C_m$ | mean piston speed (m/s) |
| $CR$ | compression ratio |
| $c$ | specific heat (J/kg-K) |
| $h$ | heat transfer coefficient ($W/m^2$-K) |
| $k$ | thermal conductivity (W/m-K) |
| $m$ | mass (kg) |
| $m_a$ | air mass in the cylinder (kg) |
| MFB | mass fraction burned (%) |
| $N$ | total harmonic number |
| $n$ | Harmonic number |
| $P$ | pressure ($N/m^2$) |
| $Q$ | heat (J) |
| $q$ | instantaneous heat flux ($W/m^2$) |
| $R$ | gas constant (kJ/kg-K) |
| $S$ | stroke |
| $S_t$ | Stanton number |
| $T$ | temperature (K) |
| $t$ | time (s) |
| $u$ | turbulent fluctuating velocity (m/s) |
| $V$ | volume ($m^3$) |
| $x$ | distance (m) |
| $\alpha$ | thermal diffusivity ($m^2/s$) |
| $\gamma$ | the ratio of specific heats |
| $\eta_v$ | volumetric efficiency |
| $\theta$ | crank angle (°) |
| $\theta_0$ | start of combustion timing (°) |
| $\theta_d$ | total combustion duration (°) |
| $\rho$ | gas density ($kg/m^3$) |
| $\tau$ | time period of the temperature (s) |
| $\omega$ | angular speed (rad/s) |

*Subscripts*

| | |
|---|---|
| *ai* | airflow into the intake manifold |
| *ao* | airflow out of the intake manifold |
| *cyl* | cylinder |
| *d* | displacement |
| *e* | engine |
| *f* | fuel |
| *g* | gas |
| *HV* | heating value |
| *ht* | heat transfer |
| *hr* | heat release |
| *im* | intake manifold |
| *m* | mean value |
| *p* | piston |
| *sp* | spark plug |
| *w* | wall |

$$\frac{dQ_{ht}}{dt} = hA(T_g - T_{sp}) \tag{1}$$

where $A$ is the area of the heat transfer surface, which is two times the piston area, i.e. $2A_p$, for obtaining global heat transfer rate [7]; $h$ is the empirical heat transfer coefficients, which is assumed the same for the entire heat transfer surface [8–11]; $T_{sp}$ is the measured temperature of the spark plug temperature; and $T_g$ is the temperature of the flowing gas, which can be obtained using the state equation of ideal gas [7,9,12] as follows:

$$T_g = \frac{P_{cyl}V_{cyl}}{m_a R} \tag{2}$$

where $P_{cyl}$ is the cylinder gas pressure, $V_{cyl}$ is the cylinder volume, $m_a$ is the air mass in the cylinder, and $R$ is the gas constant.

In order to provide a simple heat transfer model, but yet accurate enough, for the engine simulation, a heat transfer coefficient using the Stanton number $S_t$ is proposed in this paper, as follows:

$$h = S_t \rho c_p u \tag{3}$$

where $u$ is the gas turbulent fluctuating velocity, which can be approximated as $0.5C_m$ under the assumption of open combustion chamber without swirl [9]. The factor $c_p$ is the specific heat at constant pressure, and can be expressed as:

$$c_p = \frac{R}{1 - (1/\gamma)} \tag{4}$$

where $\gamma$ is the specific heat ratio, which can be obtained using the following equation [13]:

$$\gamma = 1.338 - 6 \times 10^{-5} T_g + 10^{-8} T_g^2 \tag{5}$$

The Stanton number $S_t$, which is proposed by previous study of Wu et al. [7] based on Suzuki AN125 scooter engine (as Table 1), is determined as a function of the mean piston speed $C_m$ and is expressed as

$$S_t = 0.718 \exp(-0.145 C_m) \tag{6}$$

**Table 1**
Specifications of the target engines.

| | | |
|---|---|---|
| Engine model | Suzuki AN125 | SYM CB125 |
| Engine type | Four-stroke, air cooled, OHC | |
| Bore × stroke | 52.0 × 58.6 mm | 56.5 × 49.5 mm |
| Fuel system | Carburetor | |
| Number of valves | 2 | |
| Displacement volume | 125 c.c. | |
| Compression ratio | 10.2 | 9.1 |
| Idle speed | 1800 rpm | |
| Ignition type | CDI | |
| Spark advance | 5°/1500 rpm, 26°/ 4500 rpm | 7°/1500 rpm, 23°/ 4500 rpm |
| Cylinder head material | Aluminum alloy | |
| Combustion chamber | Hemisphere shaped | |

Since Eq. (6) was proposed based on single engine, it may not be so accurate for other engines. Another heat transfer model also using Stanton number is developed in this paper.

## 3. Heat flux analysis

### 3.1. Experimental setup

Two 125 c.c. four-stroke air-cooled spark-ignition engines with single cylinder were employed for developing the heat transfer coefficient in this paper, with specifications as shown in Table 1. Moreover, the combustion chambers of both engines are hemisphere-shaped, as shown in Fig. 1.

Five thermocouples were used to measure the temperatures of the cylinder head at specific positions, as shown in Fig. 2 and Table 2. Two E-type coaxial thermocouples (Medtherm TCS-102-E), $th_1$ and $th_2$, were used to measure the instantaneous temperatures of the inside surface of the cylinder wall near the exhaust and intake valves, respectively. The E-type thermocouples offer measurement ranges from −270 to +1000 °C and temperature tolerance of

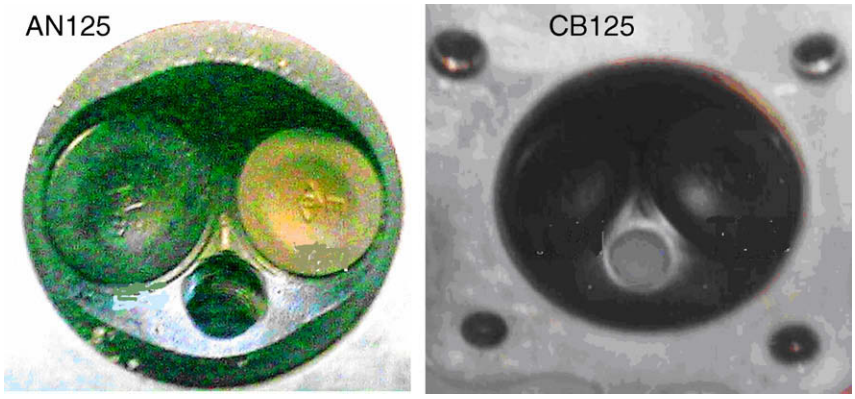


**Fig. 1.** Combustion chambers of both engines.

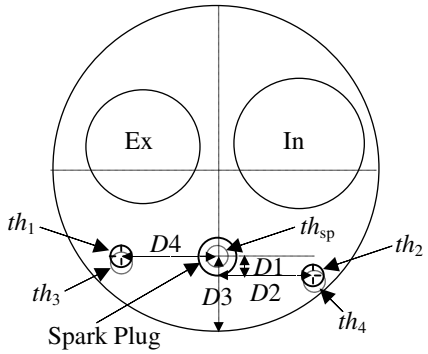


**Fig. 2.** Inside view of the locations of thermocouples.

**Table 2**
Detail location of thermocouples.

| | Suzuki AN125 | SYM CB125 |
|---|---|---|
| *D*1 (mm) | 3 | 3 |
| *D*2 (mm) | 7 | 9 |
| *D*3 (mm) | 5 | 6 |
| *D*4 (mm) | 8 | 9 |

*Note:* *D*1 is the distance between the $th_{sp}$ and the spark plug. *D*2 is the distance from the $th_{2,4}$ to the spark plug. *D*3 is the distance between the spark plug and cylinder wall. *D*4 is the distance from the $th_{1,3}$ to the spark plug.

±1.7 °C or 0.75% [14]. Two K-type thermocouples with Omega 650 temperature indicator, $th_3$ and $th_4$, were used to measure the steady-state temperatures of the outside surface of the cylinder wall near the exhaust and intake valves, respectively. Another K-type thermocouple, $th_{sp}$, was used to measure the temperature of the spark plug $T_{sp}$. The K-type thermocouples offer measurement ranges from −270 to +1372 °C and temperature tolerance of ±2.2 °C or 0.75% [14]. Moreover, since the measuring probe of E-type and K-type thermocouples are very small, the sizes are 1/32 and 1/16 inch, respectively, which can minimize the error of measured temperature.

The mean cylinder gas temperature $T_g$ was estimated using the state equation of ideal gas as shown in Eq. (2) with the cylinder pressure, which was measured with the spark-plug type pressure transducer (Kistler 6117A37).

In order to obtain the engine heat transfer rate for a wide-range of operating conditions, the engine speed was adjusted from 3000 to 6000 rpm at increments of 1000 rpm, and the brake mean effective pressure (BMEP) used as the engine load was adjusted from 1 to 7 bar with an increment of 1 bar.

### 3.2. Heat flux calculation

In most heat flux calculation, the heat flux through the cylinder head wall is assumed to be one-dimensional unsteady heat conduction [1,4,9–11]. Since the unsteady heat conduction of the in-wall temperature field exists only within a very small distance from the wall surface, the unsteady component of the temperature gradient perpendicular to the surface is usually much larger than that parallel to the surface. Therefore, one-dimensionality is safely assumed for the unsteady component of the surface heat flux calculation [10]. The heat flux at the combustion chamber can be obtained by solving the following partial differential equation with two boundary conditions:

$$\frac{\partial T}{\partial t} = \alpha \frac{\partial^2 T}{\partial^2 x} \tag{7}$$

where $T$ is the temperature of the cylinder wall, which is a function of $t$ and $x$; $t$ is the time; $x$ is the distance from the wall surface; $\alpha = k/\rho c$ is the thermal diffusivity; $k$ is the thermal conductivity; and $c$ is the specific heat. The boundary conditions are defined as follows:

$$\begin{aligned} T(0,t) &= T_{wi}(t) \quad \text{at} \quad x = 0 \\ T(\ell,t) &= T_{wo}(t) = \text{constant} \quad \text{at} \quad x = \ell \end{aligned} \tag{8}$$

where $T_{wi}$ is the instantaneous temperature of the cylinder inside wall surface and $T_{wo}$ is the steady-state temperature of the cylinder outside wall surface with a distance $\ell$ from the inside wall surface. The material properties of the cylinder head with $k$ and $\alpha$ are functions of temperature [15], as shown in Fig. 3.

First, $T_{wi}$ is represented by the following Fourier series [16]:

$$T_{wi} = T_{wm} + \sum_{n=1}^{N} [A_n \cos(n\omega t) + B_n \sin(n\omega t)] \tag{9}$$

where $T_{wm}$ is the time-averaged value of $T_{wi}$; $\omega$ is the angular frequency of temperature variation, which is one half of the engine

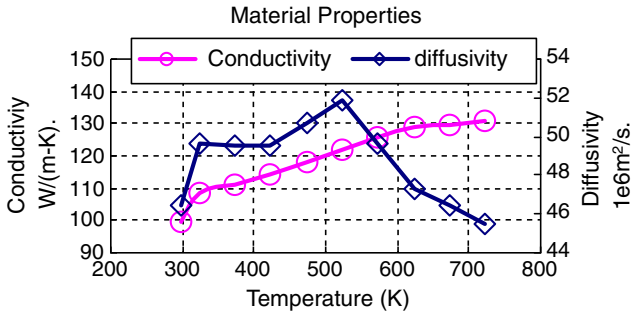


**Fig. 3.** Material thermal properties [15].

angular velocity for the four-stroke engine; and $N$ is the harmonic number which is set to be 200 in this paper for obtaining more accurate representation without more computation time [7].

The solution of Eq. (7) can be expressed as

$$T(x,t) = T_{wm} - (T_{wm} - T_{wo}) + \sum_{n=1}^{\infty} e^{-c_n x} F_n(x,t) \tag{10}$$

where

$$F_n = A_n \cos(n\omega t - c_n x) + B_n \sin(n\omega t - c_n x) \tag{11}$$

$$A_n = \frac{2}{\tau}\int_0^{\tau} T_w(t)\cos(\omega n t)dt \tag{12}$$

$$B_n = \frac{2}{\tau}\int_0^{\tau} T_w(t)\sin(\omega n t)dt \tag{13}$$

$$c_n = \sqrt{\frac{n\omega}{2\alpha}} \tag{14}$$

The instantaneous heat flux at the cylinder inside wall surface, i.e. $x = 0$, can then be obtained using Fourier's law, as follows:

$$\begin{aligned} q_w(t) &= -k\left(\frac{\partial T}{\partial x}\right)_{x=0} \\ &= \frac{k}{\ell}(T_{wm} - T_{wo}) + k\sum_{n=1}^{N} c_n[(A_n + B_n)\cos(n\omega t) \\ &\quad + (B_n - A_n)\sin(n\omega t)] \end{aligned} \tag{15}$$

Since the major heat flux is produced within compression and expansion strokes, $q_w$ is calculated only for these two strokes. The measured temperatures of the cylinder inside wall surface for AN125 and CB125 at 6000 rpm with 7 bar BMEP are shown in Figs. 4 and 5, respectively.

As can be seen from Figs. 4 and 5, the temperature near the exhaust valve $T_{wi,ex}$ is higher than that near the intake valve $T_{wi,in}$, because the exhaust valve region is heated by the high-temperature exhaust. Both $T_{wi,ex}$ and $T_{wi,in}$ have large temperature gradients near TDC due to the combustion. Since the compression ratio of AN125 is larger than that of the CB125, which results in higher combustion temperature, as well as cylinder inside wall temperature.

The corresponding instantaneous heat fluxes $q_{w,ex}$ and $q_{w,in}$ of AN125 and CB125 can then be calculated for the exhaust and intake valve regions, respectively, as shown in Figs. 6 and 7. The greater the temperature gradient, the higher the heat flux is.

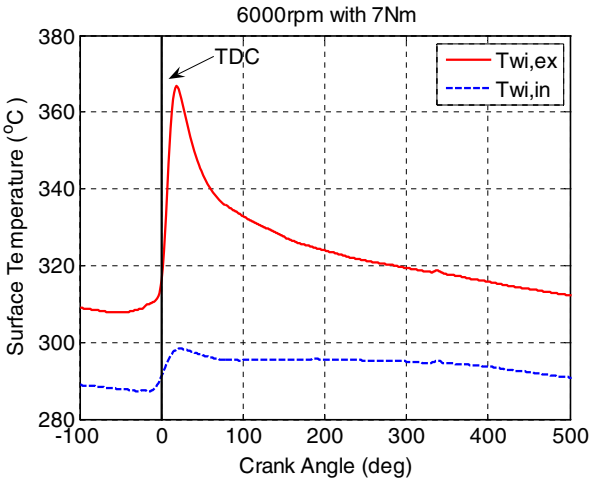


**Fig. 4.** Temperature variation of the cylinder inside wall surface for AN125.

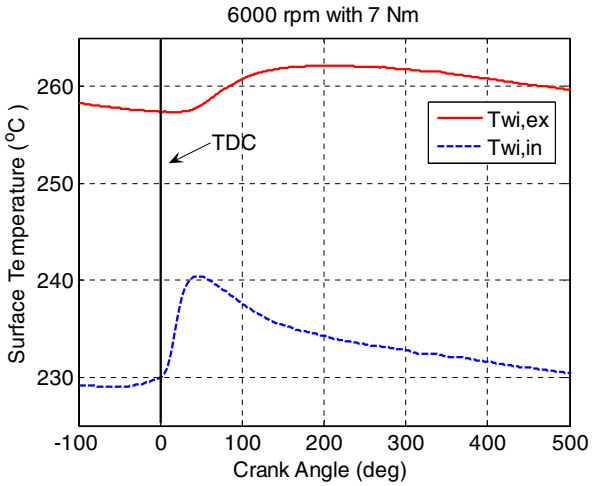


**Fig. 5.** Temperature variation of the cylinder inside wall surface for CB125.

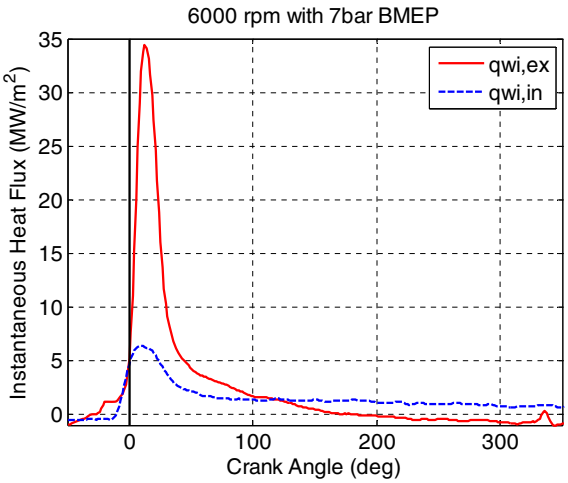


**Fig. 6.** Instantaneous heat flux variation of the cylinder inside wall surface for AN125.

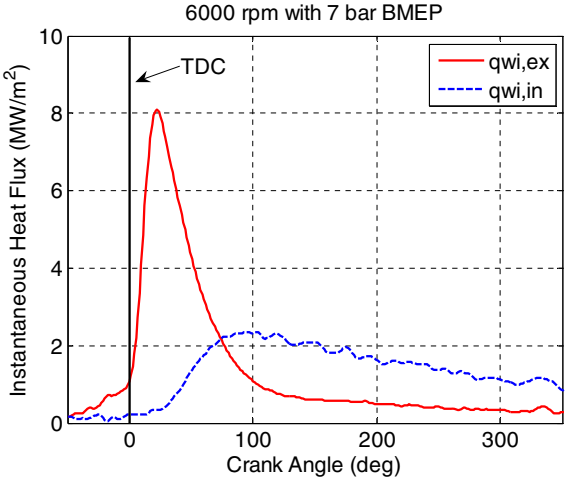


**Fig. 7.** Instantaneous heat flux variation of the cylinder inside wall surface for CB125.

Two instantaneous heat fluxes at the exhaust and intake valve regions are used to represent the average instantaneous heat flux

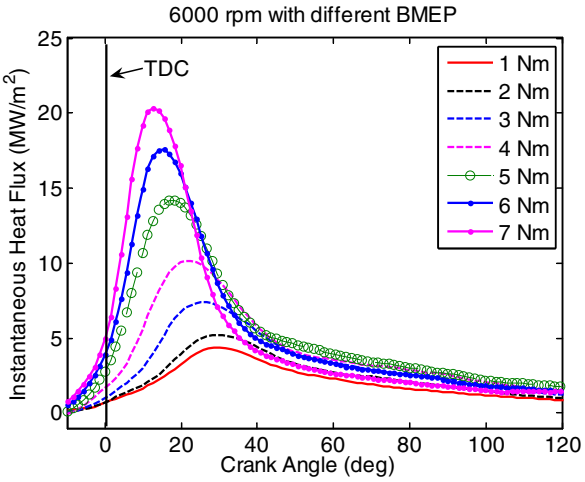


**Fig. 8.** Heat flux with various engine loads at 6000 rpm for AN125.

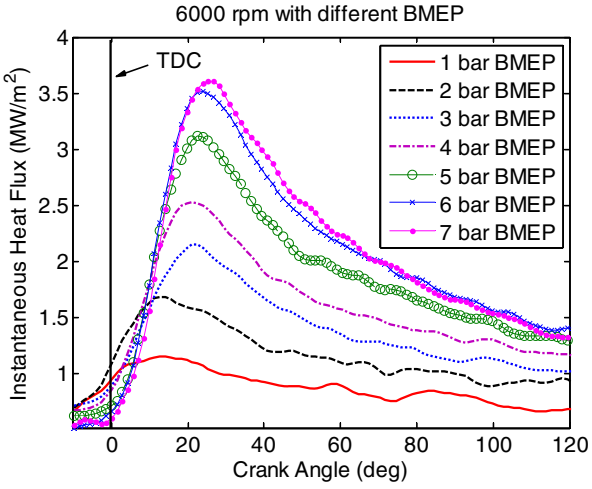


**Fig. 9.** Heat flux with various engine loads at 6000 rpm for CB125.

$q_m$, i.e. $q_m = (q_{w,in} + q_{w,ex})/2$. Figs. 8 and 9 show the experimental results of AN125 and CB125 with various load conditions at 6000 rpm. The instantaneous heat flux grows with increasing engine load, due to the gas heat transfer coefficient is increased with higher gas pressure and temperature [11,17]. Figs. 10 and 11 show the experimental results of AN125 and CB125 with different engine speeds at 6 bar BMEP. Since the gas pressure and temperature do not vary significantly with the engine speed under constant load, the gas heat transfer coefficient changes only slightly with various engine speeds, as does the instantaneous heat flux.

### 3.3. Curve fitted heat flux

For the engine simulation, the heat transfer rate can be obtained using Eq. (1). In order to develop the proposed heat transfer model, the spark plug temperature is assumed to be $T_{sp}$ in this paper. Since $T_{sp}$ cannot be measured during simulation, the previous study [7] proposed an experimental formula, which is defined as a function of engine speed and intake manifold pressure, to represent the response of $T_{sp}$. However, the previous proposed $T_{sp}$ is developed based on single engine, i.e. AN125, it may not be suitable for other engines. Thus, another experimental formula is proposed for $T_{sp}$ in this paper, and is determined as a function of intake manifold pressure $P_{im}$, engine speed $\omega_e$, and compression ratio $CR$, as follows:

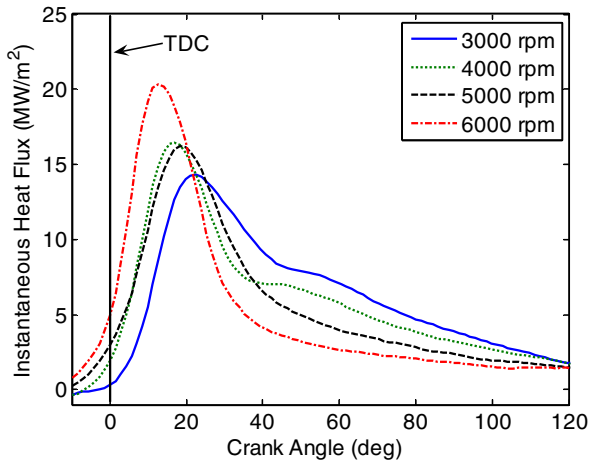


**Fig. 10.** Heat flux with various engine speeds at 6 bar BMEP for AN125.

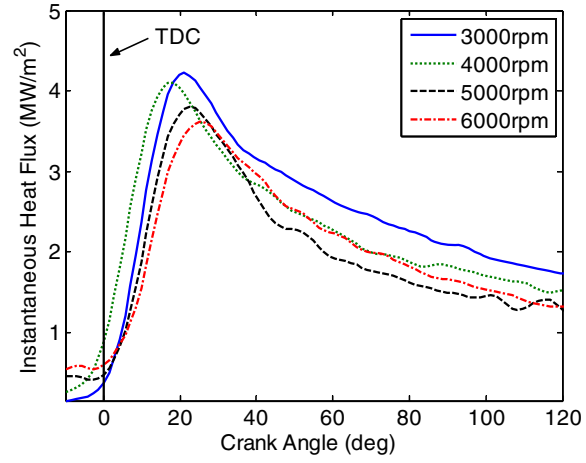


**Fig. 11.** Heat flux with various engine speeds at 6 bar BMEP for CB125.

$$T_{sp} = a_{sp1}\omega_e + a_{sp2}\omega_e^2 + a_{sp3}P_{im} + a_{sp4}\omega_e P_{im} + a_{sp5}P_{im}^2 + a_{sp6}CR \tag{16}$$

where $\omega_e$ is the engine speed with the unit of rev/sec; $P_{im}$ is the intake manifold pressure with the unit of bar; and $a_{spi}$ is the coefficient obtained from the curve fitting of experimental results and is listed in Appendix A; The coefficient of determination $R_S$ is used to evaluate correlations between the measured and predicted values of $T_{sp}$. $R_S$ can be expressed as

$$R_S = \frac{\sum_{i=1}^{n}(\hat{y}_i - \bar{y})^2}{\sum_{i=1}^{n}(y_i - \bar{y})^2} \tag{17}$$

where $y$ is the experimental data; $\bar{y}$ is the mean value of experimental data; and $\hat{y}$ is the predicted data. Here, $R_S$ ranges between 0 and 1. If $R_S$ is close to 1, the curve fitted result is close to actual value, and vice versa. The correlation results of AN125 and CB125 are shown in Fig. 12 and Table 3. Since $R_S$ of the proposed model for the AN125 and CB125 are equal to 0.9667 and 0.9736, respectively, the predicted results are determined to be very close to the experimental data than the previous model.

In order to develop a heat transfer model for all operating conditions of two target engines, the Stanton number $S_t$ is also employed for the proposed model, and can be obtained from the curve fitting of the experimental heat transfer coefficient using the following equation:

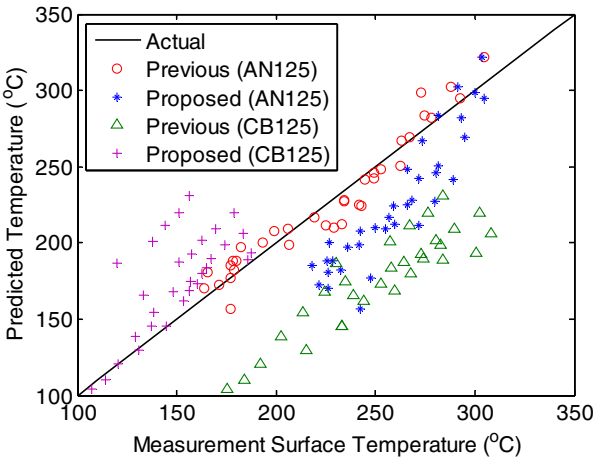


**Fig. 12.** Correlations between the measured and predicted $T_{sp}$ for AN125 and CB125.

**Table 3**
$R_S$ of predicted $T_{sp}$.

| | Previous | Proposed |
|---|---|---|
| AN125 | 0.9959 | 0.9983 |
| CB125 | 0.1496 | 0.9965 |
| Average | 0.5727 | 0.9974 |

$$h = \frac{q_m}{T_g - T_{sp}} \tag{18}$$

As can be seen from Figs. 13 and 14, the Stanton number of the AN125 and CB125 are varied with engine speed, and presents an exponential tendency. Therefore, this paper employed an exponential function with the engine speed to represent the dynamics of Stanton number. Moreover, since the characteristic of heat transfer would be affected by engine geometry, such as compression ratio $CR$, stroke $S$, displaced cylinder volume $V_{cyl}(\theta)$. Thus the $S_t$ can be expressed as follows:

$$S_t = 5.91488CR \cdot S^2\left[0.0089(10^5 V_{cyl}(\theta))^2 + \exp(-0.0106C_m^2)\right] \tag{19}$$

where the displaced cylinder volume $V_{cyl}(\theta)$ is a function of crank angle $\theta$.

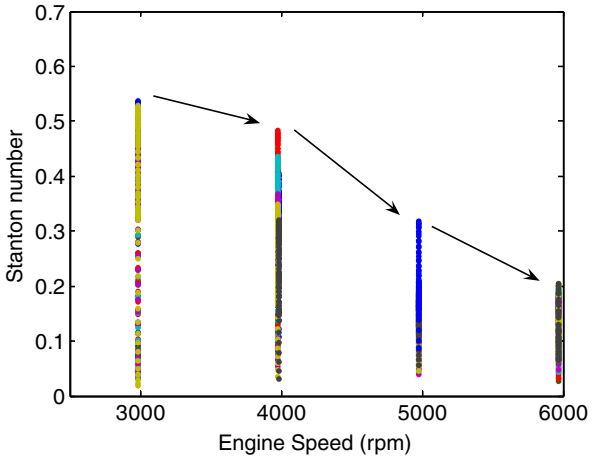


**Fig. 13.** Correlations of experimental Stanton number of AN125 and engine speed.

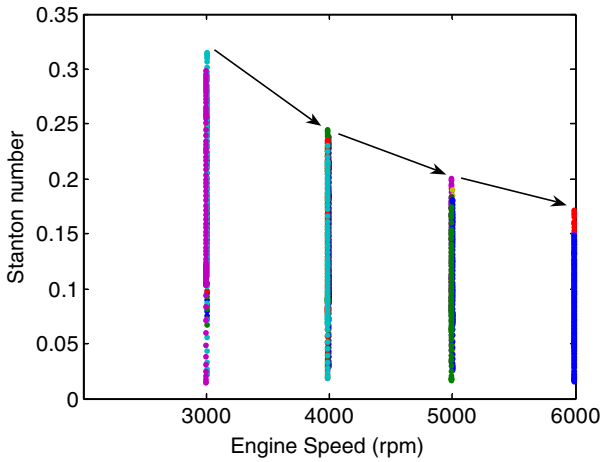


**Fig. 14.** Correlations of experimental Stanton number of CB125 and engine speed.

The correlations between the predicted and measured instantaneous heat flux for AN125 and CB125 are shown in Figs. 15 and 16, respectively. The corresponding results of $R_S$ for AN125 and CB125 are shown in Table 4. Since the previous model is developed based on AN125, its prediction results are close to experimental data than proposed model. But the averaged $R_S$ of the proposed model for both engines has larger $R_S$ than previous one, i.e. the proposed model has more accurate prediction results than previous one about 30.3%.

Similar correlation results for the heat transfer at the cylinder head of AN125 and CB125 are shown in Figs. 17 and 18. The proposed model for both engines has closer prediction results than previous one, about 83.6%. As can be seen from Table 5, since the $R_S$ of proposed model for both engines are very close to 1, the predicted results of the proposed model are determined to be very close to experimental data.

In general, the heat release rate between the intake valve closed (IVC) and spark advance (SA) angle ($\dot{Q}_{hr,IVC\to SA}$) should close to zero, due to that the combustion chamber is a closed system and the fuel energy is not released yet. Thus, this characteristic is employed to evaluate the proposed model. The heat release rate can be obtained using the experimental data of the cylinder pressure, and can be expressed as follows:

$$\frac{dQ_{hr}}{d\theta} = \frac{c_v}{R}\left(p\frac{dV_{cyl}}{d\theta} + V_{cyl}\frac{dP_{cyl}}{d\theta}\right) + P_{cyl}\frac{dV_{cyl}}{d\theta} + \frac{dQ_{ht}}{d\theta} \tag{20}$$

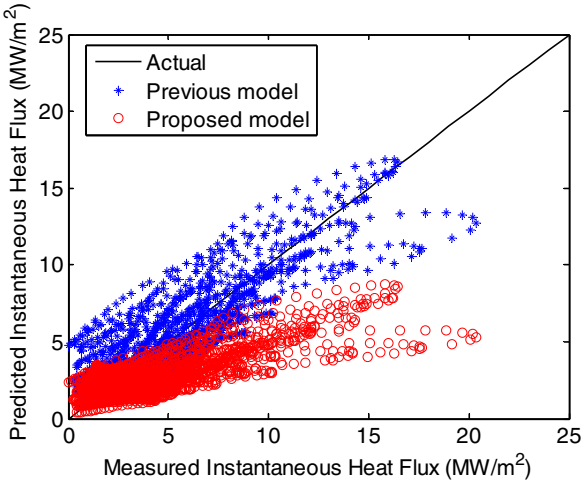


**Fig. 15.** Correlation between the predicted and measured instantaneous heat flux for AN125.

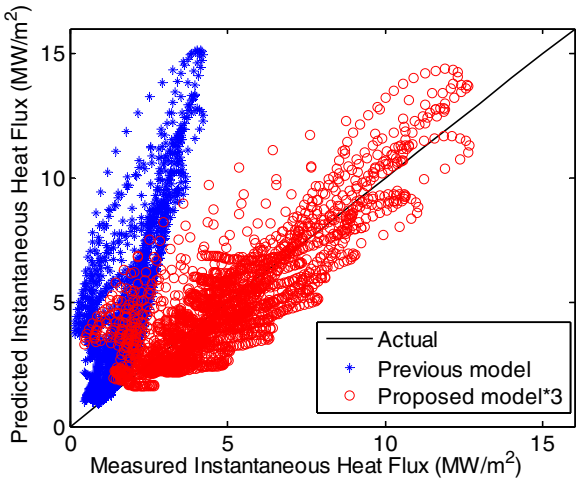


**Fig. 16.** Correlation between the predicted and measured instantaneous heat flux for CB125.

**Table 4**
$R_S$ of instantaneous heat flux.

| | Previous | Proposed |
|---|---|---|
| AN125 | 0.998 | 0.378 |
| CB125 | 0.052 | 0.989 |
| Average | 0.525 | 0.684 |

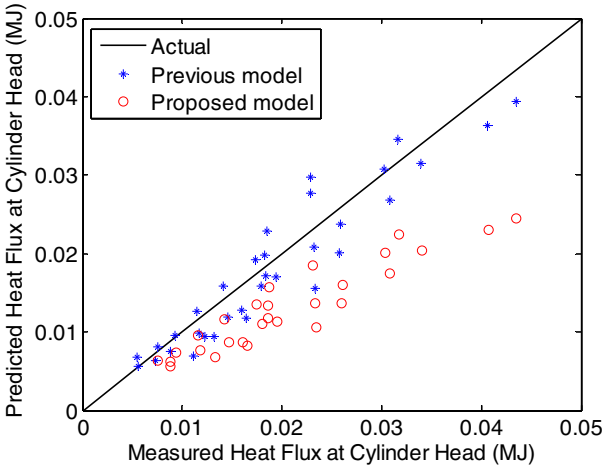


**Fig. 17.** Correlation between the predicted and measured heat transfer at cylinder head for AN125.

Experimental data of cylinder pressure of AN125 and CB125 are used to estimate the heat release rate. The IVC and SA of AN125 are 325° and 270°, respectively. The calculated heat release rate of AN125 with the proposed model at 3000 rpm with 6 bar BMEP is shown in Fig. 19. As can be seen from Fig. 19, the $\dot{Q}_{hr,IVC\rightarrow SA}$ of proposed model is close to zero, and its mean value of $\dot{Q}_{hr,IVC\rightarrow SA}$ is −0.287. Thus, the proposed heat transfer model has accurate estimation results between the IVC and SA.

For the CB125, the IVC and SA are 320° and 260°, respectively. The calculated heat release rate of CB125 with the proposed model at 3000 rpm with 6 bar BMEP is shown in Fig. 20. Similar to the previous calculated results, the $\dot{Q}_{hr,IVC\rightarrow SA}$ of the proposed model is also close to zero. Furthermore, the $\dot{Q}_{hr,IVC\rightarrow SA}$ of proposed model at 3000 rpm is −0.320. Thus, the proposed model also has accurate estimation results between the IVC and SA.

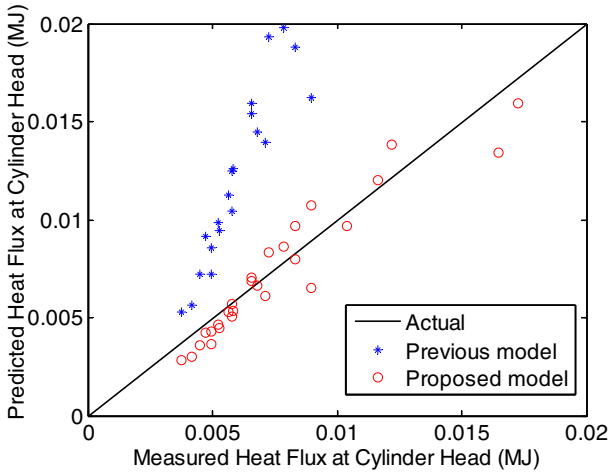


**Fig. 18.** Correlation between the predicted and measured heat transfer at cylinder head for CB125.

**Table 5**
$R_S$ of heat transfer at cylinder head.

| | Previous | Proposed |
|---|---|---|
| AN125 | 0.998 | 0.997 |
| CB125 | 0.063 | 0.952 |
| Average | 0.531 | 0.975 |

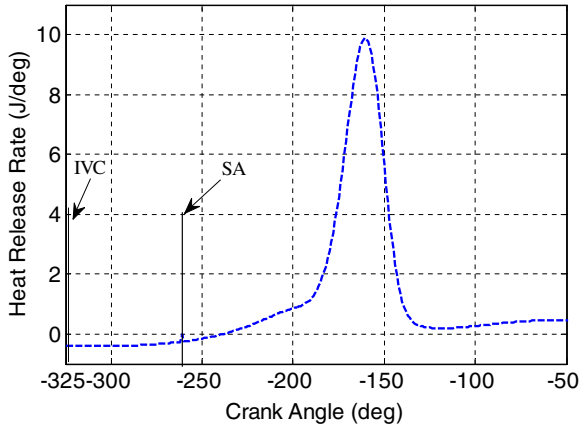


**Fig. 19.** The heat release rate of AN125 with the proposed model at 3000 rpm with 6 bar BMEP.

In order to evaluate the proposed model can be used for other operating conditions, the cylinder pressure of both engines are utilized to calculate heat release rate from 3000 to 6000 rpm with the BMEP from 2 to 7 bar. The calculated results of $\dot{Q}_{hr,IVC\rightarrow SA}$ are shown in Table 6, which shows that the proposed model can be used for overall engine operating conditions, and its root mean square of $\dot{Q}_{hr,IVC\rightarrow SA}$ is 0.403.

The results of $\dot{Q}_{hr,IVC\rightarrow SA}$ at all operating conditions of CB125 are shown in Table 7, which also shows that the proposed model has accurate estimation results between the IVC and SA for overall engine operating conditions, and its root mean square of $\dot{Q}_{hr,IVC\rightarrow SA}$ is 0.502.

## 4. Engine model

An engine model, which is consisted of charging, combustion, and rotational dynamics, is established with Matlab/Simulink as shown in Fig. 21 [18,19].

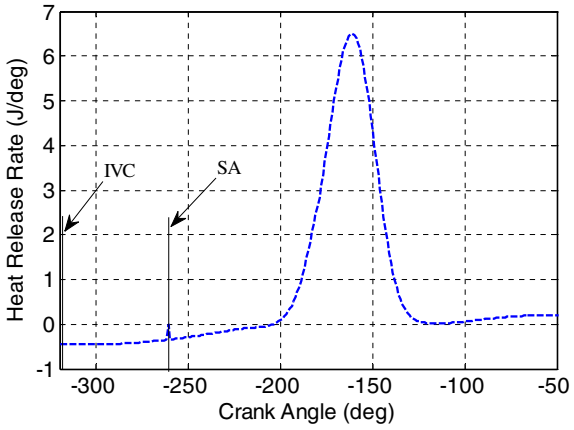


**Fig. 20.** The heat release rate of CB125 with the proposed model at 3000 rpm with 6 bar BMEP.

**Table 6**
Heat release rate $\dot{Q}_{hr,IVC\to SA}$ of AN125.

| $\omega_e$ | BMEP | | | | | |
|---|---|---|---|---|---|---|
| | 2 bar | 3 bar | 4 bar | 5 bar | 6 bar | 7 bar |
| 3000 rpm | −0.444 | −0.415 | −0.28 | −0.193 | −0.287 | 0.35 |
| 4000 rpm | −0.257 | −0.219 | −0.165 | −0.124 | 0.23 | 0.107 |
| 5000 rpm | −0.186 | −0.13 | −0.84 | −0.38 | 0.39 | 0.115 |
| 6000 rpm | −0.99 | −0.65 | −0.28 | −0.15 | −0.29 | 0.57 |

*Note:* Root mean square of $\dot{Q}_{hr,IVC\to SA} = 0.403$.

**Table 7**
Heat release rate $\dot{Q}_{hr,IVC\to SA}$ of CB125.

| $\omega_e$ | BMEP | | | | | |
|---|---|---|---|---|---|---|
| | 2 bar | 3 bar | 4 bar | 5 bar | 6 bar | 7 bar |
| 3000 rpm | −0.132 | −0.930 | −0.940 | −0.400 | −0.320 | 0.161 |
| 4000 rpm | −0.147 | −0.108 | −0.920 | −0.670 | 0.494 | 0.860 |
| 5000 rpm | −0.153 | −0.135 | −0.113 | −0.610 | −0.388 | 0.120 |
| 6000 rpm | −0.151 | −0.130 | −0.117 | −0.880 | −0.360 | −0.360 |

*Note:* Root mean square of $\dot{Q}_{hr,IVC\to SA} = 0.502$.

The charge model is a filling-and-emptying model based on the isentropic compressible flow equation for predicting the air flow rate. It consists of non-choked and choked flow dynamics as shown in Eqs. (21) and (22), respectively.

$$\dot{m}_{ai} = \frac{C_{d,im}A_{th}P_{atm}}{\sqrt{R_aT_{atm}}}\left(\frac{P_{im}}{P_{atm}}\right)^{\frac{1}{\gamma_a}}\left\{\frac{2\gamma_a}{\gamma_a-1}\left[1-\left(\frac{P_{im}}{P_{atm}}\right)^{\frac{\gamma_a-1}{\gamma_a}}\right]\right\}^{\frac{1}{2}}, \quad \text{when } \frac{P_{im}}{P_{atm}} > \left(\frac{2}{\gamma_a+1}\right)^{\frac{\gamma_a}{\gamma_a-1}} \tag{21}$$

$$\dot{m}_{ai} = \frac{C_{d,im}A_{th}P_{atm}}{\sqrt{R_aT_{atm}}}\sqrt{\gamma_a}\left(\frac{2}{\gamma_a+1}\right)^{\frac{\gamma_a+1}{2(\gamma_a-1)}}, \text{when } \frac{P_{im}}{P_{atm}} \leqslant \left(\frac{2}{\gamma_a+1}\right)^{\frac{\gamma_a}{\gamma_a-1}} \tag{22}$$

where $\dot{m}_{ai}$ is the mass airflow through the throttle body; $C_{d,im}$ is the discharge coefficient of the intake manifold; $A_{th}$ is the cross-sectional area of the throttle body; $R_a$ is the ideal gas constant of air; $\gamma_a$ is the specific heat ratio of air; $T_{atm}$ and $P_{atm}$ are the temperature and pressure of the atmosphere, respectively. The intake manifold pressure $P_{im}$ is obtained from the state equation of the ideal gas.

$$\frac{dP_{im}}{dt} = \frac{R_{air}T_{im}}{V_{im}}(\dot{m}_{ai} - \dot{m}_{ao}) \tag{23}$$

where $V_{im}$ is the volume of the intake manifold. $\dot{m}_{ao}$ is the mass airflow from the intake manifold into the cylinder, which can be expressed as:

$$\dot{m}_{ao} = \frac{P_{im}V_d}{R_{air}T_{im}\pi}\omega\eta_v \tag{24}$$

where $V_d$ is the displaced cylinder volume; $\omega$ is the engine speed; and $\eta_v$ is the volumetric efficiency.

The combustion model can be represented using the heat release model, which is a zero-dimensional model based on the first law of thermodynamics [18,19].

$$\frac{dP_{cyl}}{d\theta} = \frac{\gamma_g - 1}{V_{cyl}}\left(\frac{dQ_{hr}}{d\theta} - \frac{dQ_{ht}}{d\theta}\right) - \frac{\gamma_g P_{cyl}}{V_{cyl}}\frac{dV_{cyl}}{d\theta} \tag{25}$$

where $\gamma_g$ is the specific heat ratio of cylinder gas; $P_{cyl}$ and $V_{cyl}$ are the pressure and volume of the cylinder, respectively; and $\theta$ is the crank angle. The heat transfer rate is calculated from Eqs. (1), (3) and (19). The heat release rate with respect to the crank angle can be obtained from the rate of mass fraction burned as:

$$\frac{dQ_{hr}}{d\theta} = a_1\frac{a_2+1}{\theta_d}\left(\frac{\theta-\theta_0}{\theta_d}\right)^{a_2}\exp\left[-a_1\left(\frac{\theta-\theta_0}{\theta_d}\right)^{a_2+1}\right]Q_{HV}m_f \tag{26}$$

where $m_f$ is fuel mass injected into the cylinder; $\theta_d$ is the total combustion duration expressed in crank angle; $\theta_0$ is the start of combustion; $Q_{HV}$ is the heating value of fuel; $a_1$ and $a_2$ are 5 and 2, respectively [9].

## 5. Verification results

Experimental data of cylinder pressure are used to verify the proposed engine model. The comparison of cylinder pressures for AN125 at 3000 and 6000 rpm with 6 bar BMEP (full load) are shown in Figs. 22 and 23, respectively. Although the proposed model has larger prediction error than previous one, its maximum prediction errors are about 9% and 5% for 3000 and 6000 rpm, respectively. As can be seen from Figs. 15 and 17, the proposed model underestimates the heat flux at the cylinder head, which results in overestimated cylinder pressure. Since the previous model

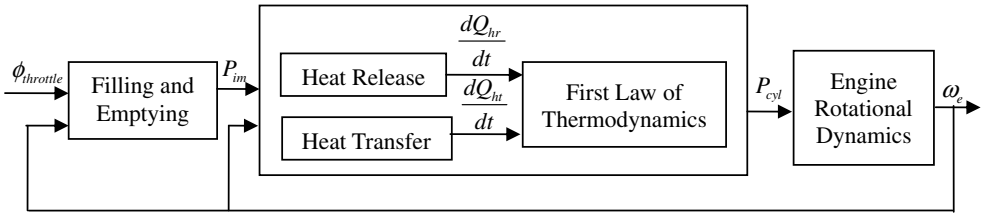


**Fig. 21.** Block diagram of the engine model.

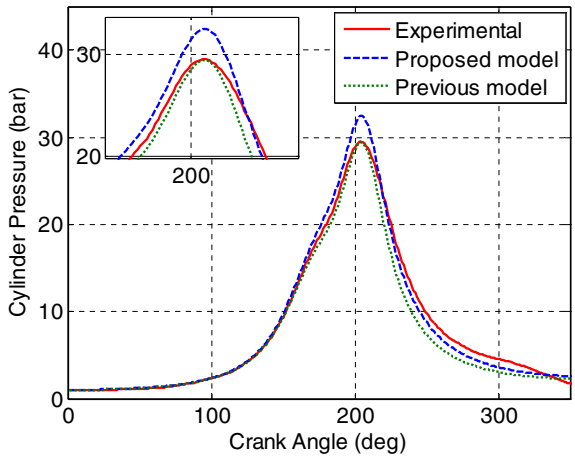


**Fig. 22.** Comparison of the cylinder pressure at 3000 rpm with 6 bar BMEP for AN125.

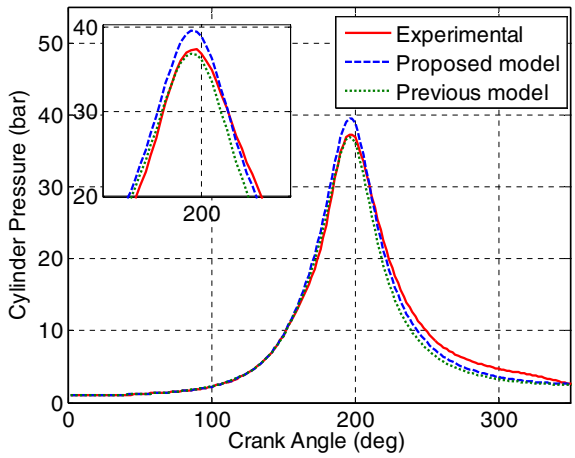


**Fig. 23.** Comparison of the cylinder pressure at 6000 rpm with 6 bar BMEP for AN125.

is developed based on AN125, its prediction results is closer to the experimental data than proposed one.

The comparison of cylinder pressures for CB125 at 3000 and 6000 rpm with 6 bar BMEP are shown in Figs. 24 and 25, respectively. Both figures show that the proposed model has the predicted results closest to the experimental data than previous one. As can been seen from Figs. 16 and 18, because the previous model overestimates the heat flux at the cylinder head significantly, which results in underestimates cylinder pressure.

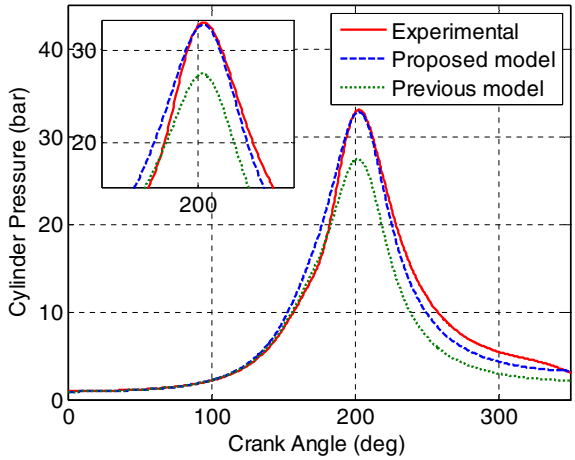


**Fig. 24.** Comparison of the cylinder pressure at 3000 rpm with 6 bar BMEP for CB125.

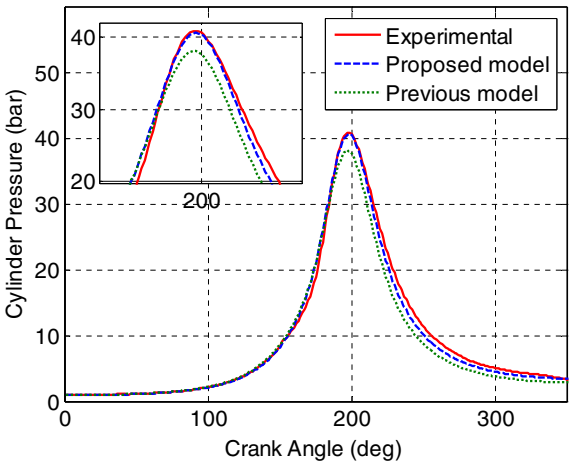


**Fig. 25.** Comparison of the cylinder pressure at 6000 rpm with 6 bar BMEP for CB125.

In order to verify the proposed model can also be used for the other engines, another experimental data of cylinder pressure (Yamaha XC125) is conducted in this paper. The specification of the XC125 is shown in Table 8.

Since the heat transfer rate is obtained based on the difference of temperature (see Eq. (1)), its estimation accuracy is significantly effected by the predicted $T_{sp}$. In order to verify the proposed $T_{sp}$ empirical formula, the experimental data of cylinder pressure (Yamaha XC125) is utilized. The correlation results of the previous empirical formula [7] and proposed one for XC125 are shown in Fig. 26. The previous formula underestimates the $T_{sp}$. The $R_S$ of the previous formula and proposed one are 0.3451 and 0.9567, respectively. Thus, the predicted results of the proposed formula are determined to be very close to the experimental data than the previous one.

Experimental data of cylinder pressure of XC125 are also used to estimate the heat release rate, and to verify the proposed heat transfer model. The IVC and SA are 310° and 265°, respectively. The calculated heat release rate of XC125 with the proposed model at 3000 rpm with 6 bar BMEP is shown in Fig. 27. Similar to the previous calculated results, the proposed model has accurate estimation results between the IVC and SA, i.e. the $\dot{Q}_{hr,IVC\to SA}$ of the proposed model is close to zero.

The cylinder pressures of XC125 at other operating conditions are also utilized to calculate $\dot{Q}_{hr,IVC\to SA}$ for evaluating the proposed

**Table 8**
Specification of the XC125.

| | |
|---|---|
| Engine model | Yamaha XC125 |
| Engine type | Four-stroke, air cooled, OHC |
| Bore × stroke | 51.5 × 60.0 mm |
| Fuel system | Carburetor |
| Number of valves | 2 |
| Displacement volume | 125 c.c. |
| Compression ratio | 10.3 |
| Idle speed | 1800 rpm |
| Ignition type | CDI |
| Spark advance | 5°/1500 rpm, 26°/4500 rpm |
| Cylinder head material | Aluminum alloy |
| Combustion chamber | Hemisphere shaped |

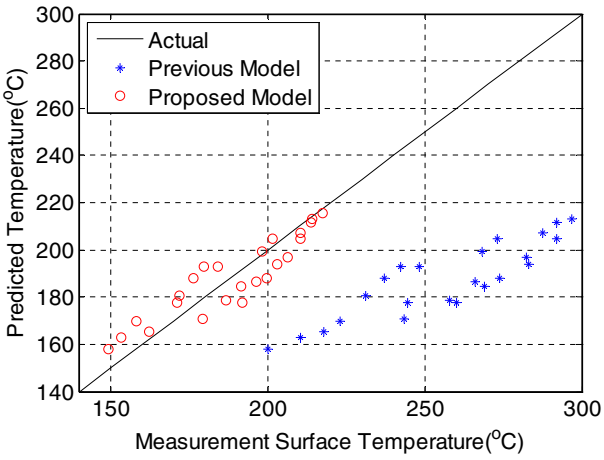


**Fig. 26.** Correlations between the measured and predicted $T_{sp}$ for XC125.

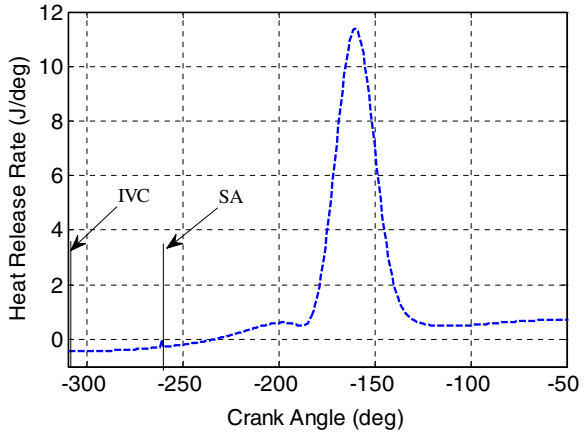


**Fig. 27.** The heat release rate of proposed model at 3000 rpm with 6 bar BMEP for XC125.

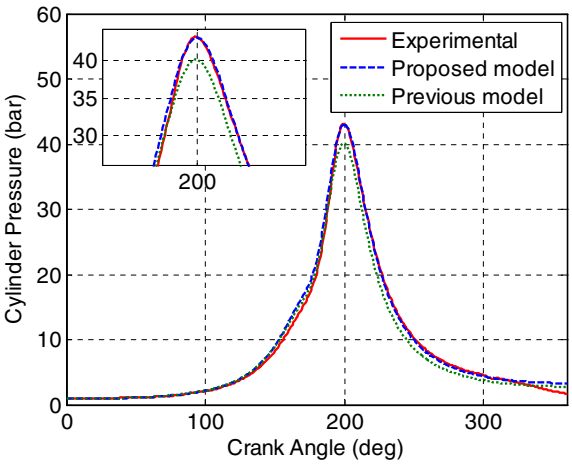


**Fig. 28.** Comparison of the cylinder pressure at 3000 rpm with 6 bar BMEP for XC125.

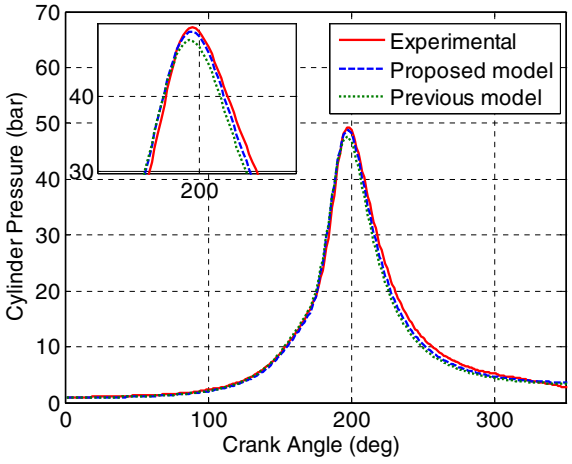


**Fig. 29.** Comparison of the cylinder pressure at 6000 rpm with 6 bar BMEP for XC125.

model. The corresponding calculated results of $\dot{Q}_{hr,IVC\to SA}$ are shown in Table 9. The proposed model also can be used for other engine operating conditions with the root mean square 0.433.

The comparison of cylinder pressures for XC125 at 3000 and 6000 rpm with 6 bar BMEP (full load) are then shown in Figs. 28 and 29, respectively. Both figures also show that the proposed model has the predicted results closest to the experimental data than previous one. Since the previous model underestimates the $T_{sp}$ (see Fig. 26), the corresponding temperature difference for calculating $dQ_{ht}/dt$ is increased, as shown in Eq. (1). Thus, it results in overestimation of cylinder pressure.

In order to compare the proposed model and previous model at all operating conditions of three engines, the difference between the $R_S$ of the proposed model $R_{S,Proposed}$ and the $R_S$ of the previous model $R_{S,Previous}$ is defined as

**Table 9**
Heat release rate $\dot{Q}_{hr,IVC\to SA}$ of XC125.

| $\omega_e$ | BMEP | | | | | |
|---|---|---|---|---|---|---|
| | 2 N | 3 N | 4 N | 5 N | 6 N | 7 N |
| 3000 rpm | −0.66 | 0.103 | 0.124 | 0.212 | −0.279 | 0.354 |
| 4000 rpm | −0.67 | −0.45 | 0.72 | 0.15 | 0.156 | 0.245 |
| 5000 rpm | −0.8 | −0.54 | −0.52 | −0.4 | 0.21 | 0.109 |
| 6000 rpm | −0.52 | −0.6 | −0.59 | −0.109 | −0.27 | 0.15 |

*Note:* Root mean square of $\dot{Q}_{hr,IVC\to SA} = 0.433$.

$$\Delta R_S = R_{S,Proposed} - R_{S,Previous} \tag{27}$$

If $\Delta R_S$ is positive, the proposed model performs better than previous one, and vice versa. The detail results of $R_S$ are shown in Appendix B. The results of $\Delta R_S$ at all operating conditions of AN125 are shown in Table 10. As can been seen from Table 10, since the previous model is developed based on AN125, it has closer prediction results than proposed model at about 62.5% of all operating conditions with a negative mean value of −0.056.

The results of $\Delta R_S$ at all operating conditions of CB125 are shown in Table 11. As can been seen from Table 11, the proposed model has the closer prediction results than previous one at most engine operation conditions about 79.2% with a positive mean value of 0.156, which is significantly larger than the negative mean value of −0.042 at the other engine operating conditions.

The results of $\Delta R_S$ at all operating conditions of XC125 are shown in Table 12, which shows that the proposed model has the closer prediction results than previous one at most engine operation conditions about 79.2% with a positive mean value of 0.066. The negative mean value is −0.067 at the other engine operating conditions.

## 6. Conclusion

The heat transfer model proposed by previous study is not so accurate for different small-scale S.I. engines because it was devel-

oped based on single engine. In order to develop a heat transfer model suitable for more small-scale S.I. engines, a heat transfer model also using the Stanton number, which is much simpler but yet accurate enough, is proposed in this paper. The proposed model is determined as a function of compression ratio, stroke, cylinder volume, and mean piston speed. Since the spark plug temperature is required for the proposed heat transfer model, an experimental formula based on two engines is proposed, and determined as a function of intake manifold pressure, engine speed, compression ratio, and throttle opening angle. Experimental data of instantaneous heat flux and global heat transfer of two engines were used to verify the proposed heat transfer model. In addition, the experimental data of cylinder pressure and corresponding heat release rate of three engines were conducted to verify the engine model with the proposed heat transfer model. The results show that the proposed model has better prediction results than the previous one at the most engine operation conditions, thus it can be widely employed for different small-scale engines.

## Acknowledgments

The authors would like to thank the Department of Industrial Technology, Ministry of Economic Affairs, of Taiwan, ROC for financial support, under Project Contract No. 95-EC-17-A-16-S1-051-B3.

## Appendix A

See Table A1.

## Appendix B

See Tables B1–B6.

**Table 10**
$\Delta R_S$ of the cylinder pressure of AN125.

| $\omega_e$ | BMEP | | | | | |
|---|---|---|---|---|---|---|
| | 2 bar | 3 bar | 4 bar | 5 bar | 6 bar | 7 bar |
| 3000 rpm | −0.011 | −0.082 | 0.007 | 0.040 | 0.089 | 0.018 |
| 4000 rpm | −0.145 | −0.193 | 0.010 | −0.025 | −0.030 | −0.014 |
| 5000 rpm | −0.123 | −0.046 | −0.015 | −0.007 | 0.009 | −0.001 |
| 6000 rpm | −0.075 | −0.068 | 0.000 | −0.001 | 0.002 | 0.008 |

*Note:* Negative mean value = −0.056; positive mean value = 0.023.

**Table 11**
$\Delta R_S$ of the cylinder pressure of CB125.

| $\omega_e$ | BMEP | | | | | |
|---|---|---|---|---|---|---|
| | 2 bar | 3 bar | 4 bar | 5 bar | 6 bar | 7 bar |
| 3000 rpm | 0.030 | 0.310 | 0.187 | 0.154 | 0.199 | 0.218 |
| 4000 rpm | 0.263 | 0.038 | −0.018 | −0.016 | 0.190 | 0.198 |
| 5000 rpm | 0.288 | 0.041 | −0.058 | 0.111 | 0.135 | 0.129 |
| 6000 rpm | 0.159 | −0.089 | −0.028 | 0.095 | 0.108 | 0.113 |

*Note:* Negative mean value = −0.042; positive mean value = 0.156.

**Table 12**
$\Delta R_S$ of the cylinder pressure of XC125.

| $\omega_e$ | BMEP | | | | | |
|---|---|---|---|---|---|---|
| | 2 bar | 3 bar | 4 bar | 5 bar | 6 bar | 7 bar |
| 3000 rpm | 0.046 | 0.101 | 0.116 | 0.142 | 0.048 | 0.119 |
| 4000 rpm | −0.046 | 0.023 | 0.128 | 0.064 | 0.013 | 0.079 |
| 5000 rpm | −0.057 | −0.080 | −0.134 | −0.020 | 0.142 | 0.005 |
| 6000 rpm | 0.095 | 0.002 | 0.015 | 0.021 | 0.047 | 0.043 |

*Note:* Negative mean value = −0.067; positive mean value = 0.066.

**Table A1**
Coefficients of $T_{sp}$.

| | |
|---|---|
| $a_{sp1}$ | −0.4375 |
| $a_{sp2}$ | −0.0128 |
| $a_{sp3}$ | −23.987 |
| $a_{sp4}$ | 0.0266 |
| $a_{sp5}$ | 0.1408 |
| $a_{sp6}$ | 111.754 |

**Table B1**
$R_s$ of cylinder pressure of the previous model for AN125.

| $\omega_e$ | BMEP | | | | | |
|---|---|---|---|---|---|---|
| | 2 bar | 3 bar | 4 bar | 5 bar | 6 bar | 7 bar |
| 3000 rpm | 0.851 | 0.962 | 0.942 | 0.903 | 0.876 | 0.971 |
| 4000 rpm | 0.960 | 0.986 | 0.988 | 0.994 | 0.999 | 0.995 |
| 5000 rpm | 0.932 | 0.928 | 0.973 | 0.984 | 0.974 | 0.998 |
| 6000 rpm | 0.936 | 0.989 | 0.954 | 0.971 | 0.973 | 0.992 |

Mean = 0.9596.

**Table B2**
$R_s$ of cylinder pressure of the proposed model for AN125.

| $\omega_e$ | BMEP | | | | | |
|---|---|---|---|---|---|---|
| | 2 bar | 3 bar | 4 bar | 5 bar | 6 bar | 7 bar |
| 3000 rpm | 0.84 | 0.8804 | 0.9486 | 0.9433 | 0.9652 | 0.9886 |
| 4000 rpm | 0.815 | 0.7926 | 0.9978 | 0.9692 | 0.9686 | 0.9814 |
| 5000 rpm | 0.8092 | 0.8824 | 0.9585 | 0.9771 | 0.9828 | 0.997 |
| 6000 rpm | 0.8613 | 0.9212 | 0.954 | 0.9706 | 0.9745 | 0.9999 |

Mean = 0.9325.

**Table B3**
$R_s$ of cylinder pressure of the previous model for CB125.

| $\omega_e$ | BMEP | | | | | |
|---|---|---|---|---|---|---|
| | 2 bar | 3 bar | 4 bar | 5 bar | 6 bar | 7 bar |
| 3000 rpm | 0.7207 | 0.6118 | 0.7039 | 0.7255 | 0.729 | 0.7427 |
| 4000 rpm | 0.6653 | 0.7837 | 0.8347 | 0.8482 | 0.7692 | 0.7893 |
| 5000 rpm | 0.6862 | 0.8247 | 0.8887 | 0.8256 | 0.8471 | 0.8526 |
| 6000 rpm | 0.7586 | 0.9061 | 0.8925 | 0.8576 | 0.874 | 0.882 |

Mean = 0.7925.

**Table B4**
$R_s$ of cylinder pressure of the proposed model for CB125.

| $\omega_e$ | BMEP | | | | | |
|---|---|---|---|---|---|---|
| | 2 bar | 3 bar | 4 bar | 5 bar | 6 bar | 7 bar |
| 3000 rpm | 0.7504 | 0.9216 | 0.8908 | 0.879 | 0.9288 | 0.9609 |
| 4000 rpm | 0.9286 | 0.8214 | 0.8172 | 0.8322 | 0.9587 | 0.987 |
| 5000 rpm | 0.9742 | 0.865 | 0.8306 | 0.9363 | 0.9821 | 0.9811 |
| 6000 rpm | 0.9173 | 0.8173 | 0.8646 | 0.9526 | 0.9819 | 0.9944 |

Mean = 0.90725.

**Table B5**
$R_s$ of cylinder pressure of the previous model for XC125.

| $\omega_e$ | BMEP | | | | | |
|---|---|---|---|---|---|---|
| | 2 bar | 3 bar | 4 bar | 5 bar | 6 bar | 7 bar |
| 3000 rpm | 0.7555 | 0.7585 | 0.7738 | 0.7884 | 0.8478 | 0.8191 |
| 4000 rpm | 0.8593 | 0.8635 | 0.8271 | 0.8769 | 0.8995 | 0.8885 |
| 5000 rpm | 0.9079 | 0.9355 | 0.9711 | 0.9119 | 0.8112 | 0.9382 |
| 6000 rpm | 0.865 | 0.9341 | 0.9259 | 0.9585 | 0.9384 | 0.924 |

Mean = 0.8742.

**Table B6**
$R_s$ of cylinder pressure of the proposed model for XC125.

| $\omega_e$ | BMEP | | | | | |
|---|---|---|---|---|---|---|
| | 2 bar | 3 bar | 4 bar | 5 bar | 6 bar | 7 bar |
| 3000 rpm | 0.8012 | 0.8593 | 0.8894 | 0.9306 | 0.8954 | 0.9383 |
| 4000 rpm | 0.8137 | 0.8866 | 0.9547 | 0.9412 | 0.9123 | 0.9679 |
| 5000 rpm | 0.8512 | 0.8554 | 0.8368 | 0.8923 | 0.9531 | 0.9436 |
| 6000 rpm | 0.9595 | 0.9355 | 0.9408 | 0.9794 | 0.9855 | 0.9673 |

Mean = 0.9121.

## References


[1] T. Oguri, On the coefficient of heat transfer between gases and cylinder walls of the spark-ignition engine, Bull. JSME 3 (11) (1960) 363–369.
[2] A.C. Alkidas, Heat transfer characteristics of a spark-ignition engine, ASME J. Heat Transfer 102 (1980) 89–193.
[3] A.C. Alkidas, J.P. Myers, Transient heat-flux measurements in the combustion chamber of a spark-ignition engine, ASME J. Heat Transfer 104 (1982) 62–67.
[4] A.C. Aldidas, I.-S. Suh, The effects of intake-flow configuration on the heat-release and heat-transfer characteristics of a single-cylinder four-valve S.I. engine, SAE Paper No. 910296, 1991.
[5] P.J. Shayler, S.A. May, T. Ma, The determination of heat transfer from the combustion chambers of si engines, SAE Paper No. 931131.
[6] A. Franco, L. Martorano, Evaluations on the heat transfer in the small two-stroke engines, SAE Paper No. 980762, 1998.
[7] Y.-Y. Wu, B.-C. Chen, F.C. Hsieh, Heat transfer model for small-scale air-cooled spark ignition four-stroke engines, Int. J. Heat Mass Transfer 49 (21–22) (2006) 3895–3905.
[8] J.L. Lumley, Engines: An Introduction, Cambridge University Press, Cambridge, 1999. pp. 95–117.
[9] J.B. Heywood, Internal Combustion Engine Fundamentals, McGraw-Hill, New York, 1988.
[10] G. Borman, K. Nishiwaki, Internal-combustion engine heat transfer, Prog. Energy Combust. Sci. 13 (1987) 1–46.
[11] W.J.D. Annand, Heat transfer in the cylinders of reciprocating internal combustion engines, Proc. Inst. Mech. Eng. 177 (36) (1963) 973–990.
[12] C.F. Taylor, The Internal Combustion Engine in Theory and Practice, vol. 1, MIT Press, Cambridge, MA, 1966. pp. 266–290.
[13] M.F.J. Brunt, H. Rai, L.A. Emtage, The calculation of heat release energy from engine cylinder pressure data, SAE Paper No. 981052.
[14] Medtherm Corporation, Product Information Coaxial Surface Thermocouple Probes, Huntsville, Alabama, USA.
[15] P. Labelle, M. Pekgularyuz, R. Bouchard, New aspects of temperature behavior of AJ52x, creep resistant magnesium alloy, SAE Paper No. 2002-01-0079.
[16] G. Lindfield, J. Penny, Numerical Methods Using Matlab, Prentice-Hall, Englewood Cliffs, NJ, 1999.
[17] C.D. Rakopoulos, G.C. Mavropoulos, D.T. Hountalas, Measurements and analysis of load and speed effects on the instantaneous wall heat fluxes in a direct injection air-cooled diesel engine, Int. J. Energy Res. 24 (7) (2000) 587–604.
[18] Y.-Y. Wu, Y. Shiao, B.-C. Chen, Motorcycle engine modeling for real time control, in: Sixth International Symposium on Advanced Vehicle Control, Hiroshima, Japan, JSAE 20024526, 2002.
[19] B.-C. Chen, Y.-Y. Wu, F.-C. Hsieh, Estimation of engine rotational dynamics using closed-loop estimator with stroke identification for engine management systems, Proc. Inst. Mech. Eng. D 219 (12) (2005) 1391–1406.